# An Analytical Solution for the SSFP Signal in MRI

Wolfgang Hänicke[1*] and Horst U. Vogel[2]

**Among previous analyses of the steady-state free-precession (SSFP) signal in rapid MRI, one treatment resulted in equations that require the evaluation of infinite binomial series. Here, an analytical solution is derived by a transformation into the power series expansion of the derivative of the inverse sine function, which is essentially a root. The treatment is extended to include higher-order signals. The results demonstrate the identity of the vastly different equations for the SSFP signals reported so far. Applications consist of the derivation of closed expressions for the signal in echo-shifted MRI and a corresponding analysis of TrueFISP sequences. Magn Reson Med 49:771–775, 2003.**


**Key words: SSFP; higher-order SSFP signals; MRI; rapid MR imaging**

The steady-state free-precession (SSFP) signal (1) was among the first NMR signals exploited for MRI in the form of the sensitive point method (2). Current MRI sequences based on the SSFP signal extract the free-induction decay (FID) part immediately following the excitation pulse (SSFP-FID), the echo part preceding the next excitation pulse (SSFP-echo), specific higher-order contributions from the signal, or use the coherent sum of all signals.

A comprehensive analysis of the SSFP signal under steady-state conditions has been given for high-resolution NMR spectroscopy (3). In the context of MRI, signal and contrast were specified for pertinent SSFP sequences (4–8). Although based on the integration of the same expression for the steady-state transverse magnetization immediately after an RF pulse (3,9,10), the use of different methods of calculation resulted in vastly different expressions, the identity of which is not readily apparent. The results from Gyngell (6) require the evaluation of infinite (though converging) summations. Therefore, certain applications using this approach for the analysis of pathologic contrast in interventional MRI (11), signal strength in echo-shifted sequences (12), and $T_2$ imaging with low specific absorption rate at high fields (13), as well as the extension to higher-order echoes (14), remain somewhat unsatisfactory.

Here, we solve these infinite sums and derive closed expressions for the different components of the SSFP signal. It is shown that for basic SSFP signals, the theories from Gyngell (6) and Zur et al. (7,8) lead to identical results. Moreover, for higher-order SSFP signals the expressions derived from reference 6 in Refs. 14 and 15 are identical to those given in Ref. 8. In addition, all expressions can be reduced to those specified by Kaiser et al. (3).

The analytical solution for the signal of the echo-shifted MRI sequence from (12) is presented, and, as another example, the TrueFISP (FIESTA, balanced FFE) sequence is analyzed using the developed framework.

## THEORETICAL CONSIDERATIONS

In general, an SSFP signal is generated by a train of RF pulses with 1) a constant flip angle $\alpha \neq 0°, \pm 180°$ (or integer multiples thereof), 2) a constant repetition time $TR > 0$, and 3) a certain degree of phase coherence or phase cycling. In the context of MRI, further requirements on the spin dephasing state apply because of the use of gradients. For a review, see e.g., Ref. 15.

### Basic SSFP-Signals

Summarizing the results of the analysis from Gyngell (6), the modulus of the steady-state signal amplitudes for the SSFP-FID at the beginning of the repetition interval, i.e., immediately after the RF excitation pulse, and for the SSFP-echo at the end of the repetition interval, i.e., immediately before the next RF excitation pulse, under conditions when higher-order signals can be neglected, are given by:

$$S(\text{SSFP-FID}) = M_0 \sin\alpha \frac{1 - E_1}{p}(u_0 - E_2 \cdot u_1) \quad [1]$$

$$S(\text{SSFP-echo}) = M_0 \sin\alpha \frac{1 - E_1}{p}(E_2^2 \cdot u_0 - E_2 \cdot u_1) \quad [2]$$

with equilibrium magnetization $M_0$, relaxation times $T_1$ and $T_2$, $E_1 = \exp(-TR/T_1)$, and $E_2 = \exp(-TR/T_2)$. The terms $u_0$ and $u_1$ are given by:

$$u_0 = 1 + \sum_{m=1}^{\infty} \binom{2m}{m} \left(\frac{q}{2p}\right)^{2m} \quad [3]$$

$$u_1 = \frac{1}{2} \sum_{m=1}^{\infty} \binom{2m}{m} \left(\frac{q}{2p}\right)^{2m-1} \quad [4]$$

with:

$$p = 1 - E_1 \cos\alpha - E_2^2(E_1 - \cos\alpha) \quad [5]$$

$$q = E_2(1 - E_1)(1 + \cos\alpha). \quad [6]$$

[1]Biomedizinische NMR Forschungs GmbH am Max-Planck-Institut für biophysikalische Chemie, Göttingen, Germany.
[2]Max-Planck-Institut für Strömungsforschung, Göttingen, Germany (retired).
Presented in part at the 10th Scientific Meeting and Exhibition of the ISMRM, Honolulu, Hawai'i, May, 2002.
*Correspondence to: Wolfgang Hänicke, Biomedizinische NMR Forschungs GmbH am Max-Planck-Institut für biophysikalische Chemie, 37070 Göttingen, Germany. E-mail: whaenic@gwdg.de
Received 14 May 2002; revised 23 October 2002; accepted 11 November 2002.
DOI 10.1002/mrm.10410
Published online in Wiley InterScience (www.interscience.wiley.com).

$\binom{n}{k}$ are binomial coefficients. It has been stated that $|p| > |q|$ for $T_1 > T_2$ (6). More generally, and using only the SSFP conditions from above, it can be shown that $p > q > 0$.

With the expansion of the binomial coefficients to real numbers a:

$$\binom{a}{k} = \frac{a(a-1)\ldots(a-k+1)}{k!} \quad [7]$$

for integers $k > 0$ and $\binom{a}{0} = 1$ (e.g., see Ref. 16), it can be shown that:

$$\left(\frac{1}{2}\right)^{2m}\binom{2m}{m} = (-1)^m\binom{-\frac{1}{2}}{m}. \quad [8]$$

Thus, Eq. [3] becomes:

$$u_0 = \sum_{m=0}^{\infty}(-1)^m\binom{-\frac{1}{2}}{m}\left(\frac{q}{p}\right)^{2m} \quad [9]$$

which is the power series expansion of the derivative of the inverse sine function, (e.g., see Ref. 16), $\frac{d(\arcsin q/p)}{d(q/p)} = 1/\sqrt{(1-q^2/p^2)}$. Accordingly, Eqs. [3] and [4] can be written as:

$$u_0 = \frac{p}{\sqrt{p^2-q^2}} \quad [10]$$

$$u_1 = \frac{p}{q}(u_0 - 1). \quad [11]$$

It can be shown that $u_0 > u_1 > 0$.

### Higher-Order SSFP Signals

Considering higher-order SSFP signals, the infinite summations in Eqs. [3] and [4] have to be generalized as follows (14,15):

$$u_n = \begin{cases} \sum_{m=0}^{\infty}\binom{2m+n}{m}\left(\frac{q}{2p}\right)^{2m+n} & \text{for } n \geq 0 \\ \sum_{m=|n|}^{\infty}\binom{2m+n}{m}\left(\frac{q}{2p}\right)^{2m+n} & \text{for } n < 0. \end{cases} \quad [12]$$

For $n = 0$, Eqs. [3] and [12] are obviously equivalent. With the addition theorem for the binomial coefficients and their symmetry property, we obtain the identity $\frac{1}{2}\binom{2m}{m} = \binom{2m-1}{m-1} = \binom{2m-1}{m}$ showing the equivalence of Eqs. [4] and [12] for $n = 1$, and $u_1 = u_{-1}$. Thus, the solutions from Eqs. [10] and [11] are valid for these cases. Moreover, with $\binom{2m+n}{m-1} = \binom{2m+n+1}{m} - \binom{2m+n}{m}$ we get the recursion:

$$u_n = \begin{cases} \frac{2p}{q}u_{n-1} - u_{n-2} & \text{for } n \geq 2 \\ \frac{2p}{q}u_{n+1} - u_{n+2} & \text{for } n \leq -2. \end{cases} \quad [13]$$

Complete induction yields $u_n = u_{-n}$ for all n. Using this symmetry and solving the recursion for $n \geq 2$ (see Appendix) reveals:

$$u_n = \left(\frac{p - \sqrt{p^2-q^2}}{q}\right)^{|n|}\cdot u_0 \quad [14]$$

$$= \left(\frac{u_1}{u_0}\right)^{|n|}\cdot u_0. \quad [15]$$

## RESULTS AND DISCUSSION

The consequences of the analytical solution for specific MRI sequences will be discussed below. At this stage, the effects of practical problems such as chemical shift differences, inhomogeneous slice profiles, spatial inhomogeneities, susceptibility differences, flow, motion, and diffusion are neglected.

### MRI Using Basic SSFP Signals

For the basic SSFP signals, we obtain the following expressions after substituting Eqs. [10] and [11] into Eqs. [1] and [2], and using $\tan(\alpha/2) = \sin\alpha/(1+\cos\alpha)$:

$$S(\text{SSFP-FID}) = M_0\tan\frac{\alpha}{2}(1 - (E_1 - \cos\alpha)\cdot r) \quad [16]$$

$$S(\text{SSFP-echo}) = M_0\tan\frac{\alpha}{2}(1 - (1 - E_1\cos\alpha)\cdot r) \quad [17]$$

with:

$$r = \frac{1-E_2^2}{\sqrt{p^2-q^2}} = \sqrt{\frac{1-E_2^2}{(1-E_1\cos\alpha)^2 - E_2^2(E_1-\cos\alpha)^2}}. \quad [18]$$

Equations [16]–[18] complete Gyngell's analysis (6) by specifying closed expressions. Equation [16] is identical to Eq. [13a] in Ref. 7 except for a factor describing the decay of the FID, and to Eq. [14] in Ref. 8. The expression $-S(\text{SSFP-echo})/E_2$ from Eq. [17] is identical to Eq. [13b] given in Ref. 7 except for a factor describing the increase of the echo, and to Eq. [15] given in Ref. 8. The sign is not important for conventional magnitude images and the factor $1/E_2$ is due to the fact that the signal amplitude is evaluated at the start of the repetition interval by Zur and at its end by Gyngell. So far, the equivalence between the two theories has only been observed in numerical comparisons (15). The present solution provides the missing analytical link. Moreover, the specified equations are identical to $d_0$ and $d_{-1}$ in Eq. [A4] given by Kaiser et al. (3).

### MRI Using Higher-Order SSFP Signals

Higher-order SSFP signals have been isolated using a stopped-pulse experiment in high-resolution spectroscopy (3) and using gradients and/or phase cycling (8,14) in MRI. In Refs. 14 and 15, the signal amplitude was specified:

$$S_n = M_0 \sin\alpha \frac{1 - E_1}{p} (u_n - E_2 \cdot u_{n+1}) \qquad [19]$$

using the notation from Eq. [12]. Substituting the solution from Eq. [15] yields:

$$S_n = \begin{cases} M_0 \sin\alpha \dfrac{1 - E_1}{p} \left(1 - E_2 \cdot \left(\dfrac{u_1}{u_0}\right)\right) \cdot \left(\dfrac{u_1}{u_0}\right)^n \cdot u_0 & \text{for } n \geq 0 \\ M_0 \sin\alpha \dfrac{1 - E_1}{p} \left(\left(\dfrac{u_1}{u_0}\right) - E_2\right) \cdot \left(\dfrac{u_1}{u_0}\right)^{|n|-1} \cdot u_0 & \text{for } n < 0 \end{cases} \qquad [20]$$

or

$$S_n = \begin{cases} \left(\dfrac{u_1}{u_0}\right)^n \cdot S_0 & \text{for } n \geq 0 \\ \left(\dfrac{u_1}{u_0}\right)^{|n|-1} \cdot S_{-1} & \text{for } n < 0. \end{cases} \qquad [21]$$

S(SSFP-FID) from Eq. [16] is identical to $S_0$, and $-$S(SSFP-echo)/$E_2$ from Eq. [17] is identical to $S_{-1}$. For all negative n, $S_n < 0$. Equation [21] is identical to Eqs. [16] and [16′] in Ref. 8, proving the equivalence of the theories for higher-order signals. Moreover, all expressions are identical to $d_p$ and $d_{-p-1}$ in Eq. [A4] in Ref. 3.

The optional use of the different formulations for the SSFP signal amplitudes defined either by Eq. [19] using the infinite series from Eq. [12] or by the analytical solution from Eq. [21], which is identical to that in Refs. 3 and 8, provides a mechanism to switch between the different theories.

### Echo-Shifted MRI Sequences

Echo-shifted (ES) MRI sequences (17) with an echo time TE > TR are used for functional MRI and for MR thermometry. According to (12), first-order SSFP signals are exploited in a certain class of ES-MRI sequences ("TR-periodic GRE") and the signal S(ES) can be written:

$$S(ES) = M_0 \sin\alpha \frac{1 - E_1}{p} E_2(TE)(u_1 - E_2 \cdot u_2) \qquad [22]$$

using the notation from Eq. [12], and $E_2(TE) = \exp(-TE/T_2)$. Substituting $u_n$ from Eq. [15] and using r from Eq. [18] results in:

$$S(ES) = M_0 \sin\alpha \frac{E_2(TE)}{q} (1 - E_1\cos\alpha + (1 - 2E_2^2) \times (E_1 - \cos\alpha) - r \cdot ((1 - E_1\cos\alpha)^2 - 2E_2^2(E_1 - \cos\alpha)^2 + (1 - E_1\cos\alpha) \cdot (E_1 - \cos\alpha))). \qquad [23]$$

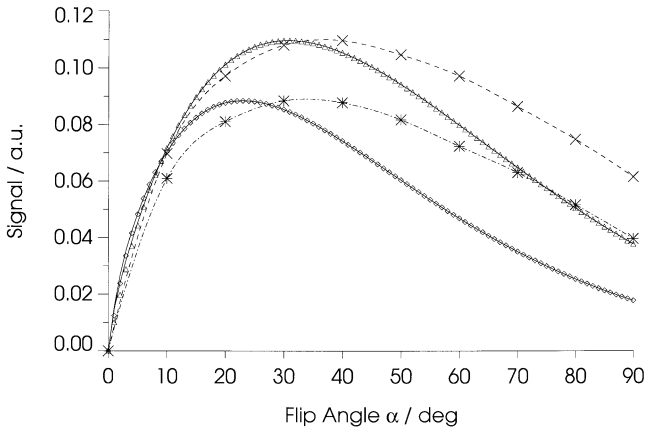


FIG. 1. Echo-shifted MRI signal as a function of flip angle α for TR/TE = 20 ms/10 ms and $T_1/T_2$ = 840 ms/400 ms (below) and 1200 ms/960 ms (above). Solid lines represent the analytical solution given in Eq. [23], diamonds (below) and triangles (above) are calculated values using the infinite sums from Eq. [22]; asterisks (interpolated by the chain-dashed line) and crosses (interpolated by the dashed line) are corresponding measured values taken from (12) and normalized for the chosen conditions.

Figure 1 shows the signal for different $T_1/T_2$ ratios and corresponding values from phantom experiments measured in Ref. 12. Small variations between the values computed from Eqs. [22] and [23] for flip angles $\alpha < 5°$ are explained by the slow convergence of the sum from Eq. [12] under these conditions and numerical problems in computing the binomial coefficients for corresponding high values of m. The remaining difference between the theoretical and measured values is explicable by the influence of slice profile deformations. Finally, it should be noted that for the Ernst angle condition, i.e., $E_1 = \cos\alpha$, the signal becomes:

$$S(ES) = M_0 \sqrt{\frac{1 - E_1}{1 + E_1}} \frac{E_2(TE)}{E_2} (1 - \sqrt{1 - E_2^2}). \qquad [24]$$

### TrueFISP MRI Sequences

TrueFISP MRI sequences (18) with extremely short repetition times find increasing applications in cardiovascular MRI (19,20). According to Ref. 15 and using $S_n$ from Eq. [19], the signal can be expressed by:

$$S(TF) = \sum_{n=-\infty}^{\infty} S_n \cdot F_n. \qquad [25]$$

$F_n$ represents the phase directly after the RF pulse. The use of Eq. [21] results in:

$$S(TF) = S_0 \cdot \sum_{n=0}^{\infty} \left(\frac{u_1}{u_0}\right)^n \cdot F_n + S_{-1} \cdot \sum_{n=0}^{\infty} \left(\frac{u_1}{u_0}\right)^n \cdot F_{-n-1}. \qquad [26]$$

For the 180° phase alternation scheme for RF excitation commonly used for TrueFISP, $F_n = (-1)^n$ applies and the use of Eqs. [10], [11], and [16]–[19] yields:

$$S(TF_{alt}) = \frac{u_0}{u_0 + u_1} \cdot (S_0 - S_{-1}) = M_0 \tan\frac{\alpha}{2}\frac{(1 + E_2)q}{E_2(p + q)} \quad [27]$$

$$= M_0 \sin\alpha \frac{1 - E_1}{1 - (E_1 - E_2)\cos\alpha - E_1E_2}. \quad [28]$$

Equation [28] is identical to Eq. [15a] in Ref. 7. For the case of RF excitation without phase cycling, i.e., $F_n \equiv 1$, we obtain:

$$S(TF_{no\ alt}) = \frac{u_0}{u_0 - u_1} \cdot (S_0 + S_{-1}) = M_0 \tan\frac{\alpha}{2}\frac{(1 - E_2)q}{E_2(p - q)} \quad [29]$$

$$= M_0 \sin\alpha \frac{1 - E_1}{1 - (E_1 + E_2)\cos\alpha + E_1E_2}. \quad [30]$$

Equation [30] is identical to Eq. [14a] in Ref. 7.

For the purpose of cardiovascular MRI, the TrueFISP sequence variant with RF phase alternation was used with TR = 3 ms and $\alpha = 60°$ (20). Assuming a $T_1$ of 1 s (at 1.5 T) and a $T_2$ of 60 ms for heart muscle (e.g., see Ref. 21), the difference between the theoretical TrueFISP signal from Eq. [28] and the coherent sum of the SSFP-FID and SSFP-echo, i.e., $S_0 - S_{-1}$ from Eq. [19], is less than 5%. Under these conditions higher-order signals can be neglected.

## CONCLUSION

In conclusion, analytical solutions are given for the infinite series in Eqs. [3], [4], and [12] allowing the solution of pertinent equations that use these series for the characterization of the different components of the SSFP signal. The resulting expressions demonstrate the identity of the different equations for SSFP signals in MRI obtained by Gyngell (6) and Zur et al. (8) and provide a mechanism to switch between their theories. Moreover, the equations from both analyses are equivalent to those obtained for high-resolution spectroscopy by Kaiser et al. (3). Closed expressions are specified for the previously published signal (12) of MRI sequences exploiting first-order SSFP signals presently used for functional MRI or MR thermometry. The signal in TrueFISP sequences as derived in closed form from the infinite series approach is shown to be identical to that obtained by Zur et al. (7).

## APPENDIX

For solving the homogeneous linear recursion from Eq. [13] we consider its characteristic (or auxiliary) equation $P(x)$ (e.g., see Refs. 22 and 23):

$$P(x) = x^n - \frac{2}{s}x^{n-1} + x^{n-2} \quad [A1]$$

$$= x^{n-2}\left(x^2 - \frac{2}{s}x + 1\right) \quad [A2]$$

with $s = q/p$. The roots of this polynomial are given by $r_{1/2} = (1/s)(1 \pm \sqrt{1 - s^2})$ with multiplicity 1 and $r_3 = 0$ with multiplicity $n - 2$. Therefore, the general solution for $u_n$ is specified by (e.g., see Refs. 22 and 23):

$$u_n = A \cdot \frac{1}{s^n}(1 - \sqrt{1 - s^2})^n + B \cdot \frac{1}{s^n}(1 + \sqrt{1 - s^2})^n. \quad [A3]$$

The constants A and B are determined by utilizing the starting conditions from Eqs. [10] and [11] for $n = 0$ and $n = 1$, resulting in the system of linear equations:

$$u_0 = A + B \quad [A4]$$

$$u_1 = \frac{1}{s}(u_0 - 1)$$

$$= A \cdot \frac{1}{s}(1 - \sqrt{1 - s^2}) + B \cdot \frac{1}{s}(1 + \sqrt{1 - s^2}) \quad [A5]$$

which is solved by $A = u_0$ and $B = 0$.

## REFERENCES


1. Carr HY. Steady-state free precession in nuclear magnetic resonance. Phys Rev 1958;112:1693–1701.
2. Hinshaw WS. Image formation by magnetic resonance: the sensitive-point method. J Appl Phys 1976;47:3709–3721.
3. Kaiser R, Bartholdi E, Ernst RR. Diffusion and field-gradient effects in NMR Fourier spectroscopy. J Chem Phys 1974;60:2966–2979.
4. van der Meulen P, Groen JP, Tinus AMC, Bruntink G. Fast field echo imaging: an overview and contrast calculations. Magn Reson Imag 1988;6:355–368.
5. Buxton RB, Fisel CR, Chien D, Brady TJ. Signal intensity in fast NMR imaging with short repetition times. J Magn Reson 1989;83:576–585.
6. Gyngell ML. The steady-state signals in short-repetition-time sequences. J Magn Reson 1989;81:474–483.
7. Zur Y, Stokar S, Bendel P. An analysis of fast imaging sequences with steady-state transverse magnetization refocusing. Magn Reson Med 1988;6:175–193.
8. Zur Y, Wood ML, Neuringer LJ. Motion-insensitive, steady-state free precession imaging. Magn Reson Med 1990;16:444–459.
9. Ernst RR, Anderson WA. Application of Fourier transform spectroscopy to magnetic resonance. Rev Sci Instrum 1966;37:93–102.
10. Freeman R, Hill HDW. Phase and intensity anomalies in Fourier transform NMR. J Magn Reson 1971;4:366–383.
11. Chung YC, Merkle EM, Lewin JS, Shonk JR, Duerk JL. Fast $T_2$-weighted imaging by PSIF at 0.2 T for interventional MRI. Magn Reson Med 1999;42:335–344.
12. Chung YC, Duerk JL. Signal formation in echo-shifted sequences. Magn Reson Med 1999;42:864–875.
13. Auerbach EJ, Heberlein K, Hu X. High-resolution, low-SAR $T_2$ imaging at high magnetic fields. In: Proc 10th Annual Meeting ISMRM, Honolulu, 2002. p 2345.
14. Mizumoto CT, Yoshitome E. Multiple echo SSFP sequences. Magn Reson Med 1991;18:244–250.
15. Scheffler K. A pictorial description of steady-states in rapid magnetic resonance imaging. Concepts Magn Reson 1999;11:291–304.
16. Bronstein IN, Semendjajew KA. Taschenbuch der Mathematik. 20. Auflage. Thun: Verlag Harri Deutsch; 1983. [English translation available as: Handbook of mathematics, 3rd ed. New York: Springer; 1997.]
17. Moonen CT, Liu G, van Gelderen P, Sobering G. A fast gradient-recalled MRI technique with increased sensitivity to dynamic susceptibility effects. Magn Reson Med 1992;26:184–189.

18. Oppelt A, Graumann R, Barfuß H, Fischer H, Hartl W, Schajor W. FISP: a new fast MRI sequence. Electromedica 1986;54:15–18.
19. Barkhausen J, Ruehm SG, Goyen M, Buck T, Laub G, Debatin JF. MR evaluation of ventricular function: true fast imaging with steady-state precession versus fast low-angle shot cine MR imaging: feasibility study. Radiology 2001;219:264–269.
20. Carr JC, Simonetti O, Bundy J, Li D, Pereles S, Finn JP. Cine MR angiography of the heart with segmented true fast imaging with steady-state precession. Radiology 2001;219:828–834.
21. Bottomley PA, Foster TH, Argersinger RE, Pfeifer LM. A review of normal tissue hydrogen NMR relaxation times and relaxation mechanisms from 1–100 MHz: dependence on tissue type, NMR frequency, temperature, species, excision, and age. Med Phys 1984;11: 425–448.
22. Biggs NL. Discrete mathematics, rev. ed. Oxford: Clarendon Press; 1989.
23. Eriksson K. A summary of recursion solving techniques. http://www.math.kth.se/~bek/diskret/linrek.pdf